Supplementary Information

Natural template derived porous carbon nanoplate architectures with tunable pore configuration for a full-carbon sodium-ion capacitor

Kunfang Wang [a], Fei Sun [a]*, Yanlin Su [a], Yingquan Chen [b], Jihui Gao [a], Haiping Yang [b], Guangbo Zhao [a]

[a] *School of Energy Science and Engineering, Harbin Institute of Technology, Harbin, 150001, China*

[b] *State Key Laboratory of Coal Combustion, Huazhong University of Science and Technology, Wuhan, 430074, China*

* Corresponding authors.

E-mail: sunf@hit.edu.cn (F. Sun).

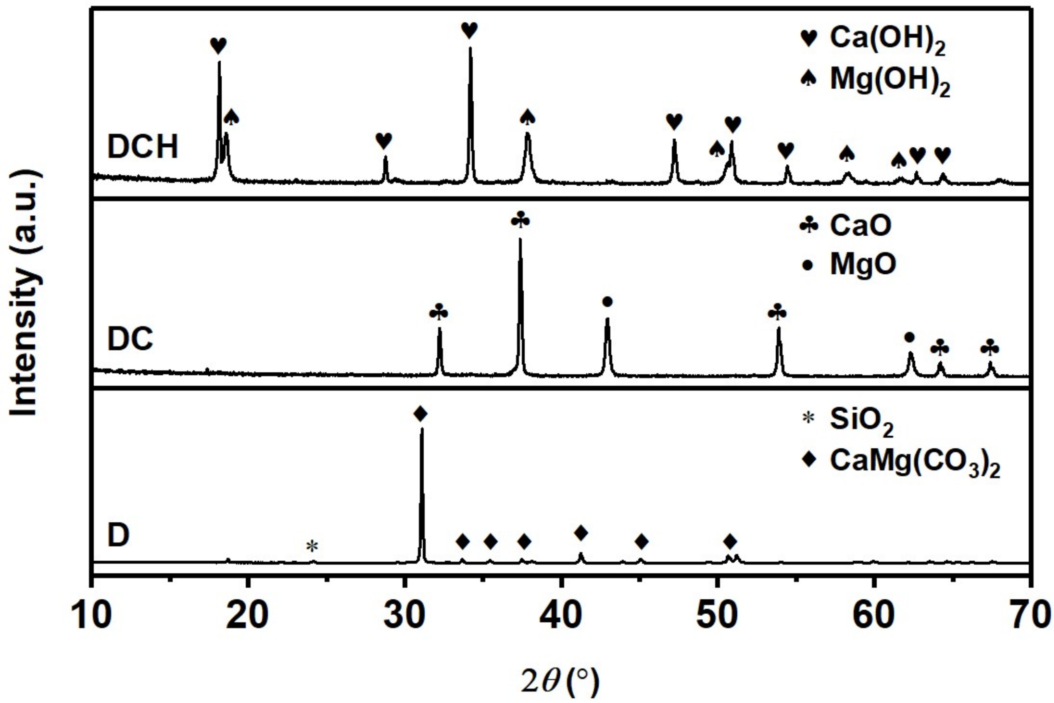

Fig. S1. XRD patterns of dolomite (D), calcined dolomite (DC) and Calcined dolomite by hydration (DCH).

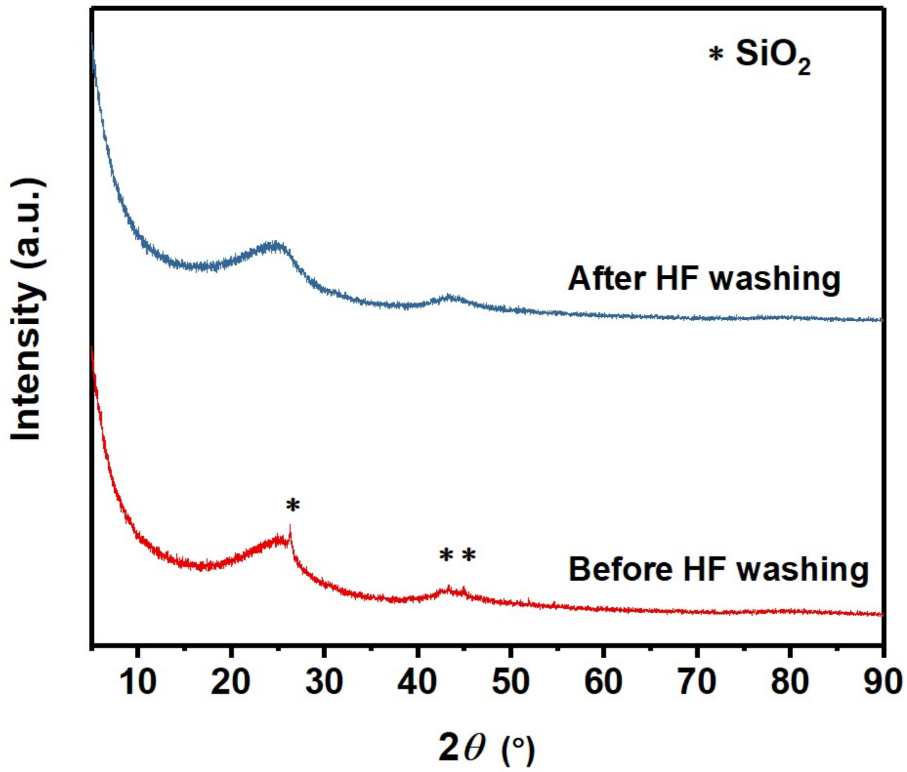

Fig. S2. XRD patterns of obtained sample before and after HF washing.

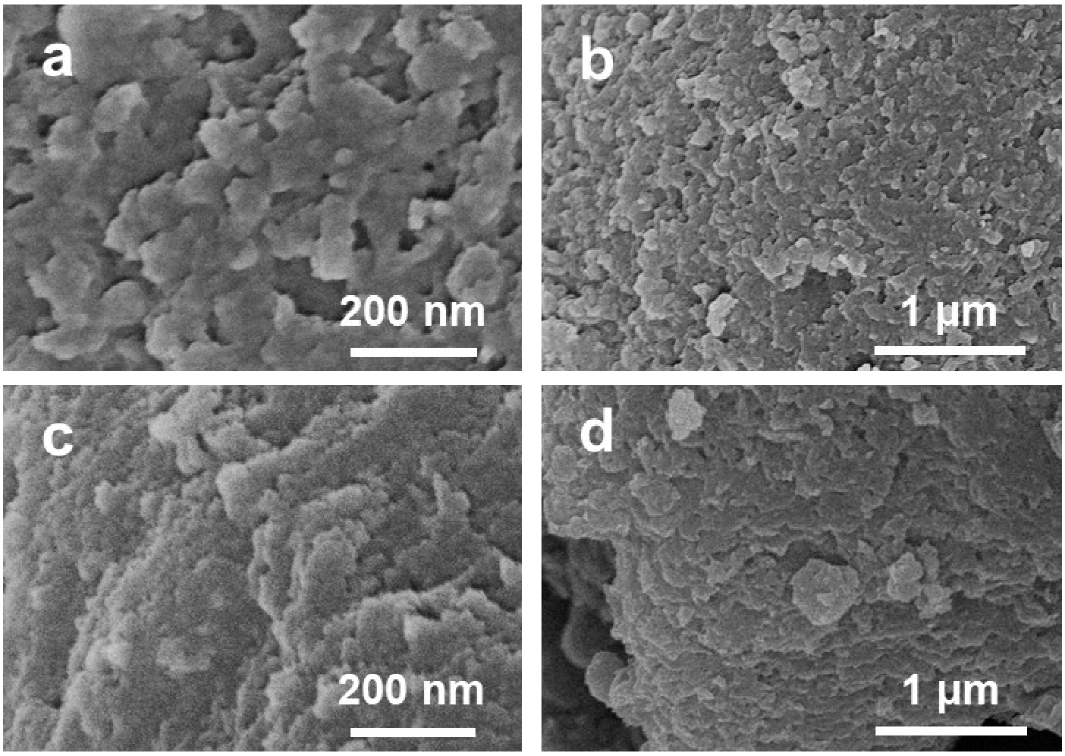

Fig. S3. SEM images of (a, b) MCNP-5 and (c, d) MCNP-10.

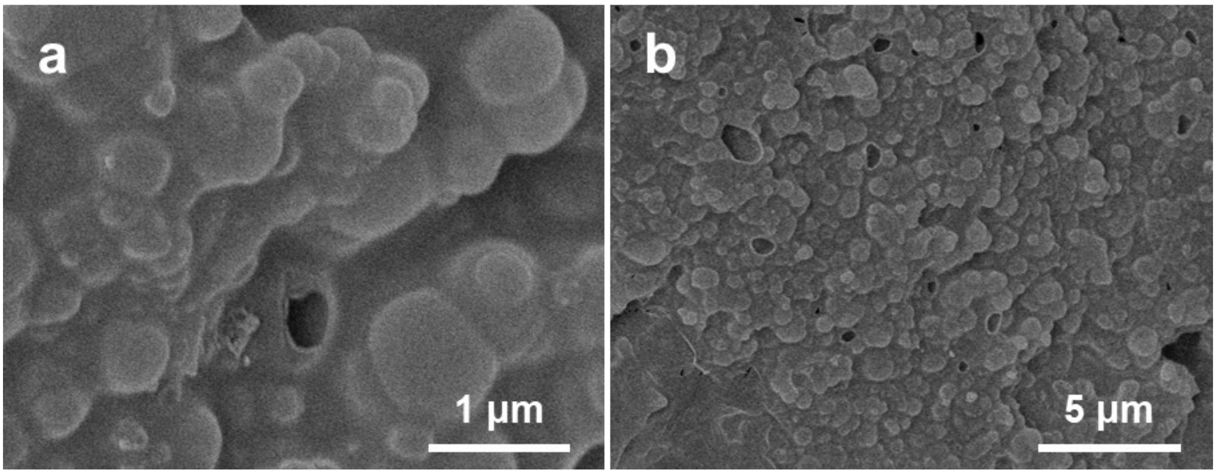

Fig. S4. SEM images of HCNP-0.

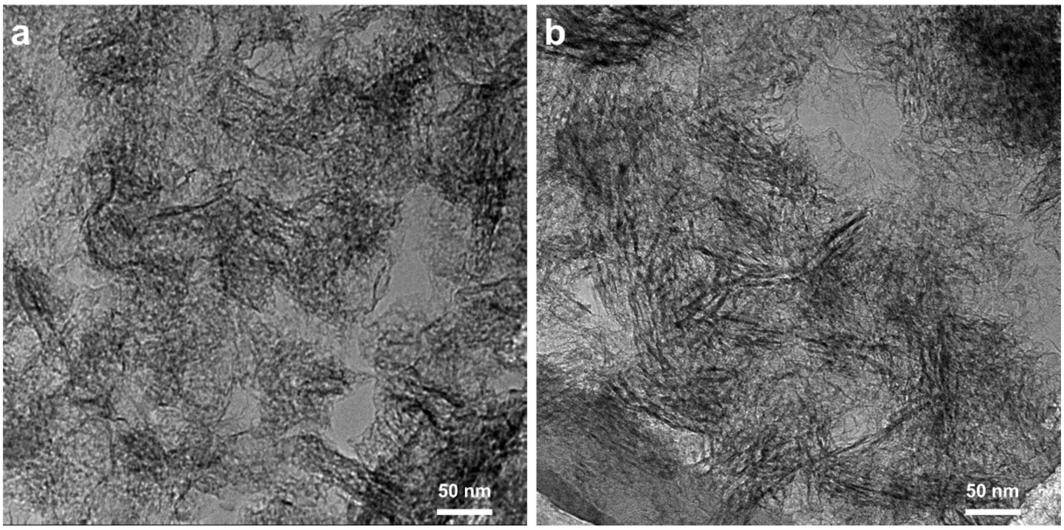

Fig. S5. TEM images of (a) MCNP-2 and (b) HCNP-2.

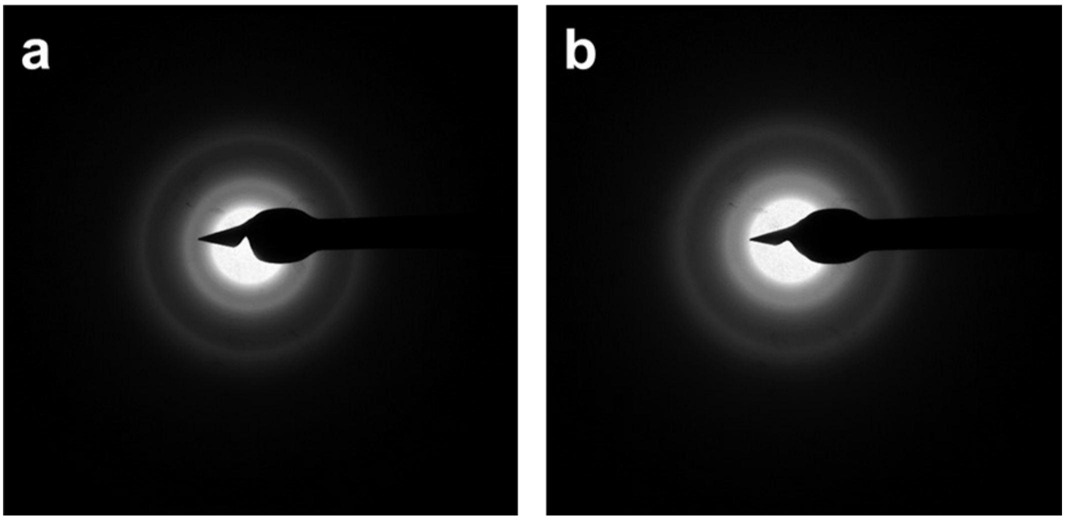

Fig. S6. SAED patterns of (a) MCNP-2 and (b) HCNP-2.

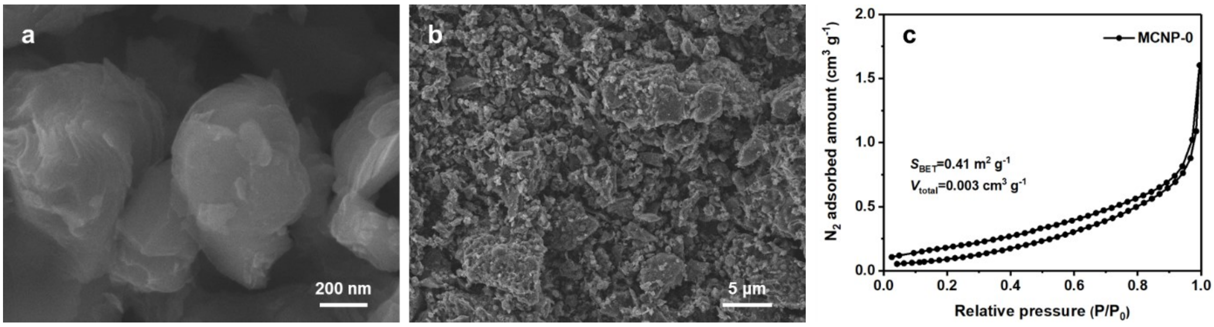

Fig. S7. (a, b) SEM images and (c) N_2 adsorption/desorption isotherm of MCNP-0**.**

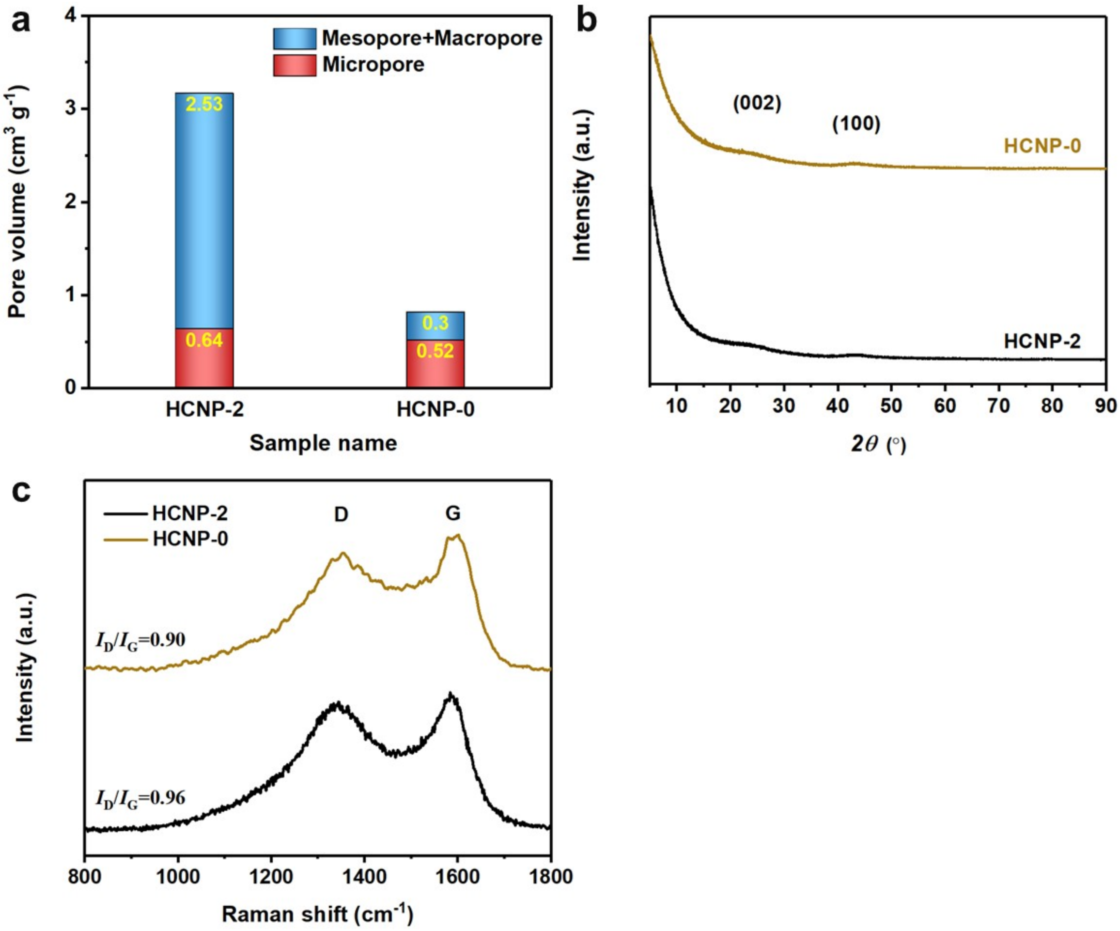

Fig. S8. (a) Pore volume distributions, (b) XRD patterns and (c) Raman spectra of HCNPs.

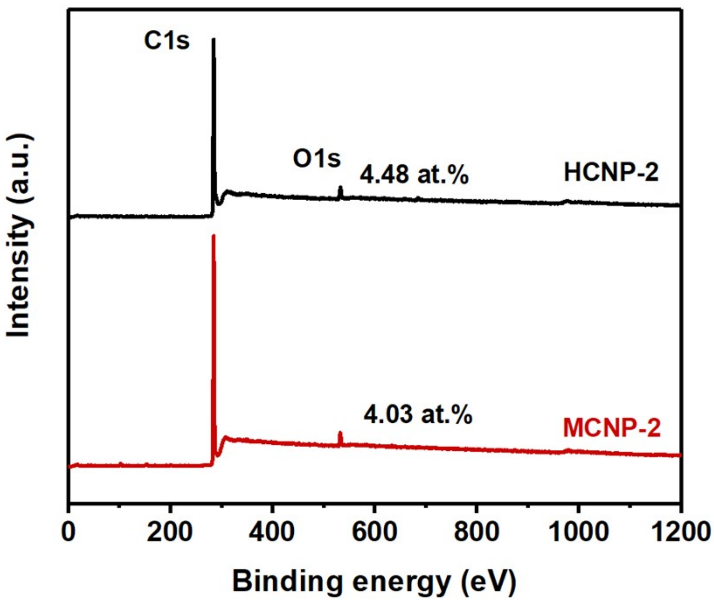

Fig. S9. XPS spectra of MCNP-2 and HCNP-2.

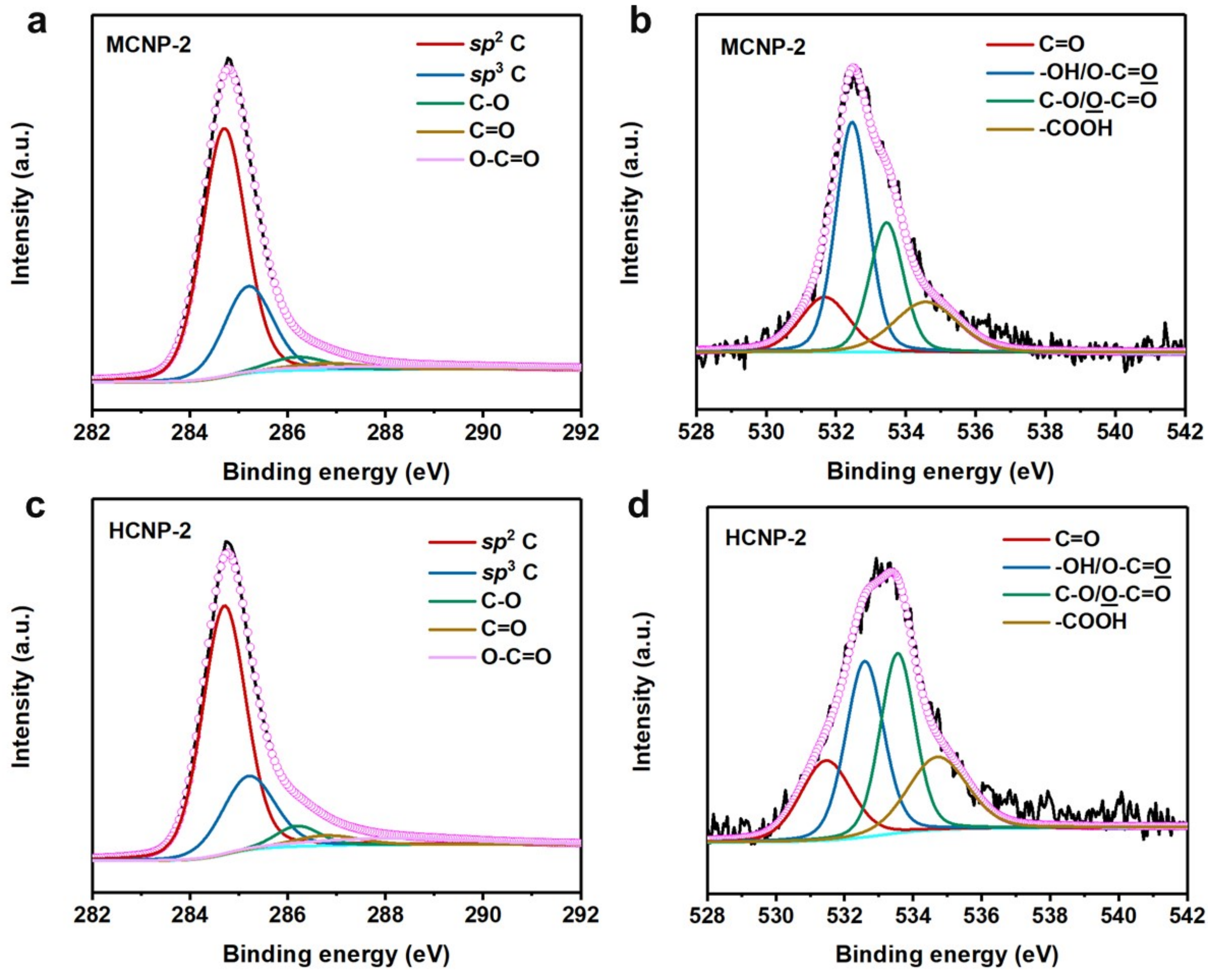

Fig. S10. The high-resolution C 1s XPS spectra of (a) MCNP-2 and (c) HCNP-2. The high-resolution O 1s XPS spectra of (b) MCNP-2 and (d) HCNP-2.

The high-resolution C 1s and O 1s spectra of MCNP-2 and HCNP-2 are shown in **Fig. S10**, which confirms that these two samples possess similar surface chemical bonds. The C 1s spectra (**Fig. S10a** and **c**) of MCNP-2 and HCNP-2 could be deconvoluted as sp^2 hybridized C=C (284.7 eV), sp^3 hybridized C-C (285.2 eV), epoxy/phenol C-O from (286.2 eV), carbonyl C=O (286.8 eV) and carboxyl O-C=O (288.7 eV) [S1]. The deconvolution of O 1s spectra of MCNP-2 and HCNP-2 in **Fig. S10b** and **d** can be split into four subpeaks, including C=O in quinone groups at 531.7 eV, oxygen atoms in hydroxyl groups (-OH) and O-C=O in esters and anhydrides groups at 532.5 eV, C-O/O-C=O in esters and anhydrides groups at 533.5 eV, and oxygen atoms in carboxyl groups (-COOH) at 534.6 eV [S2].

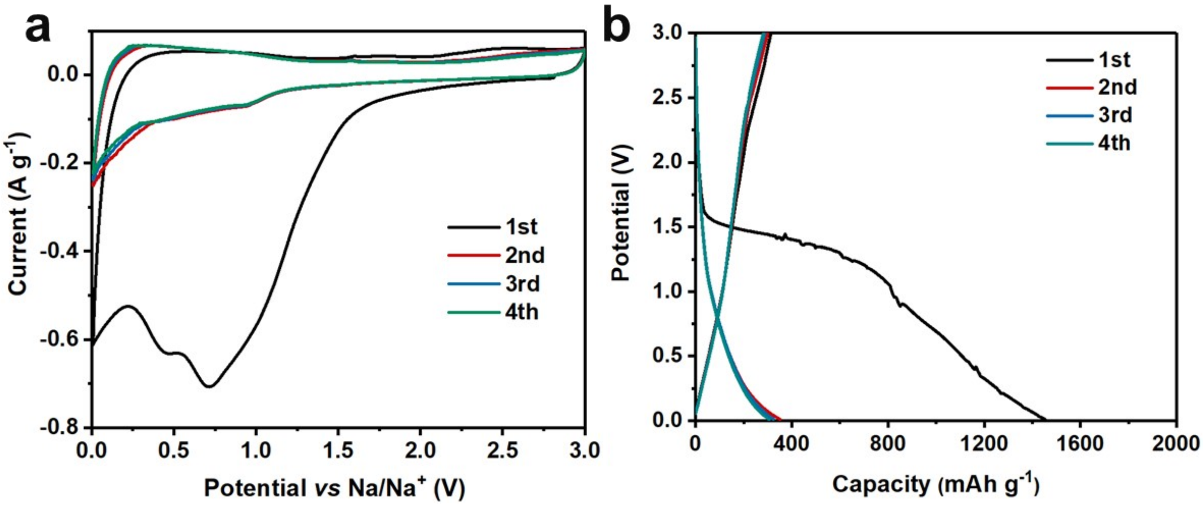

Fig. S11. (a) Initial four CV curves of MCNP-2 at the scan rate of 0.2 mV s^{-1}. (b) Initial four GCD curves of MCNP-2 at the current density of 50 mA g^{-1}.

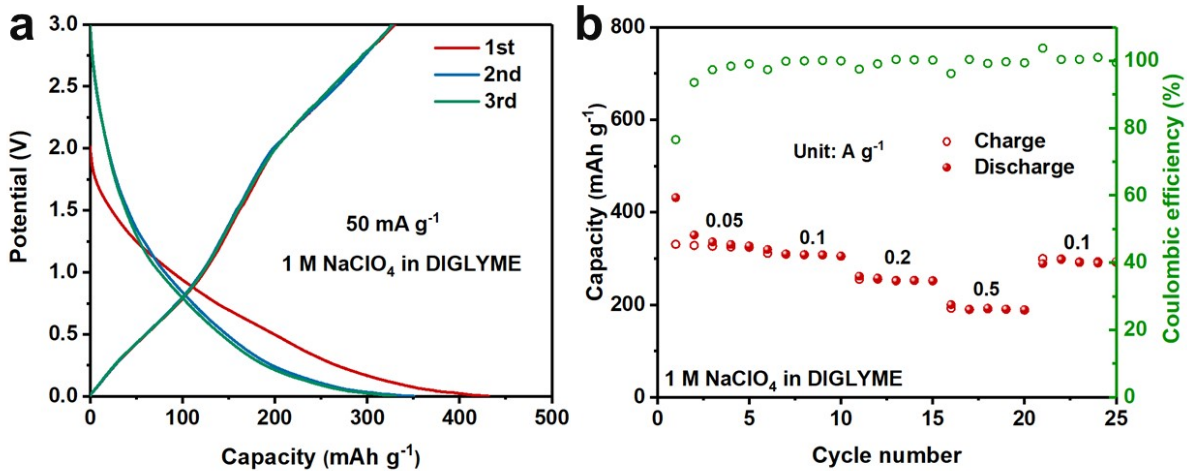

Fig. S12. (a) Initial three GCD curves and (b) rate performance of MCNP-2 in a typical ether-based electrolyte.

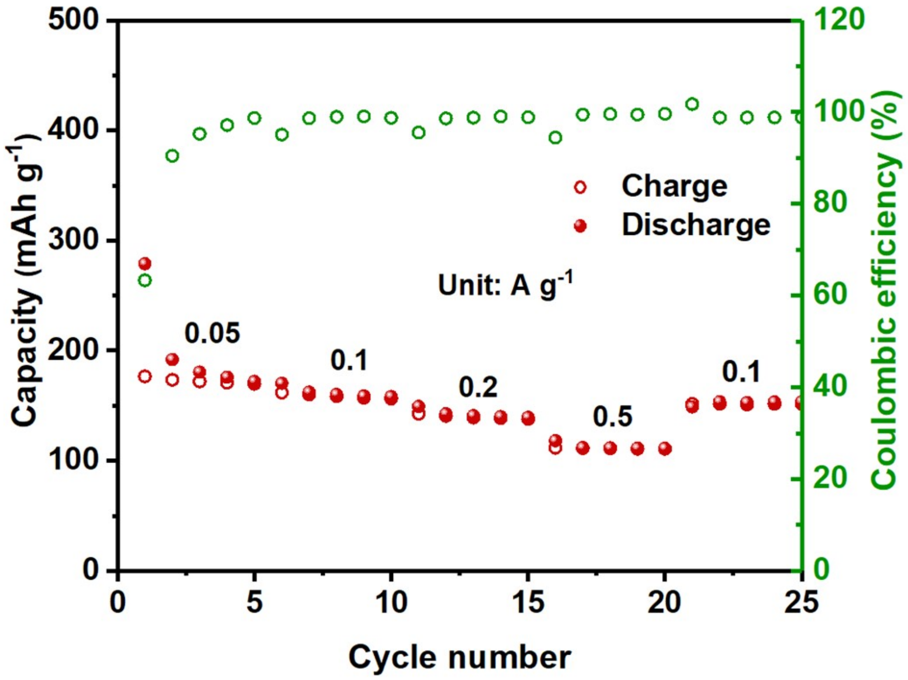

Fig. S13. Rate performance of MCNP-0.

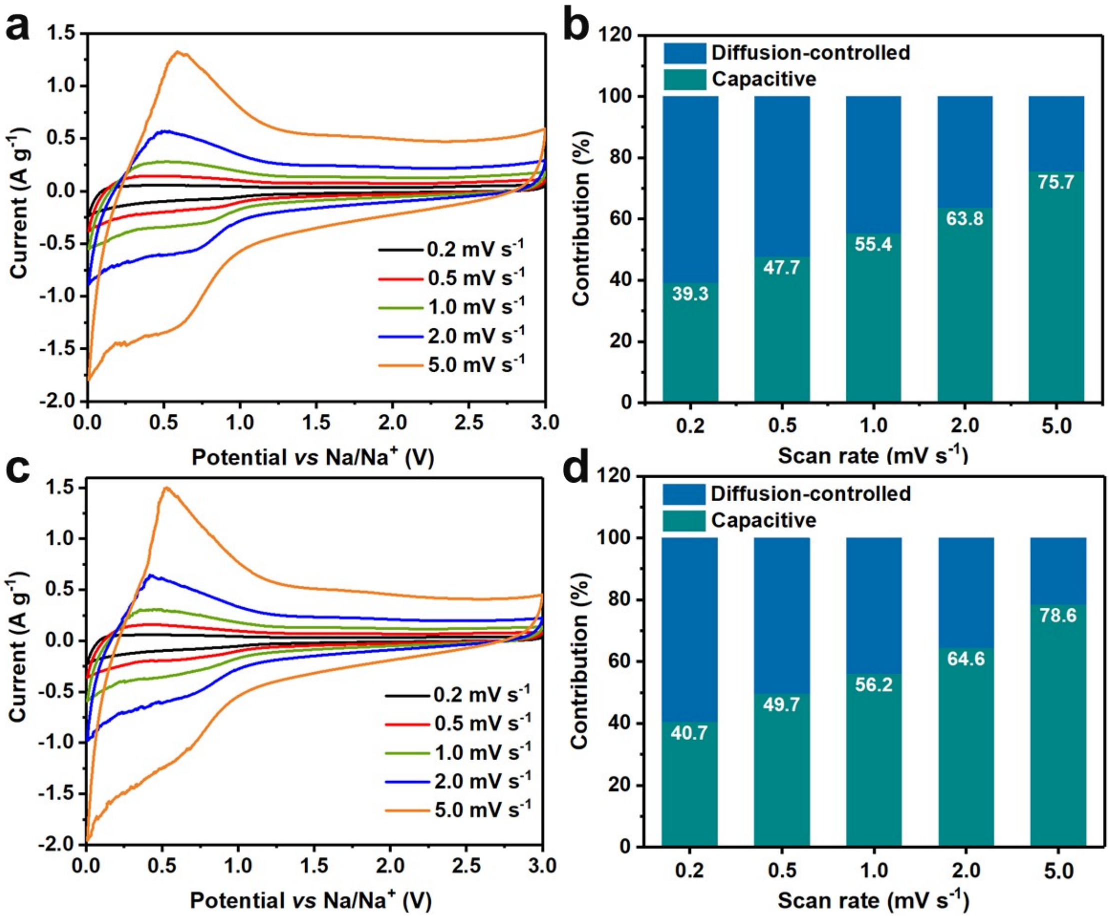

Fig. S14. CV curves of (a) MCNP-5 and (c) MCNP-10 at different scan rates. Capacity contribution of capacitive and diffusion-controlled storage at different scan rates: (b) MCNP-5, (d) MCNP-10.

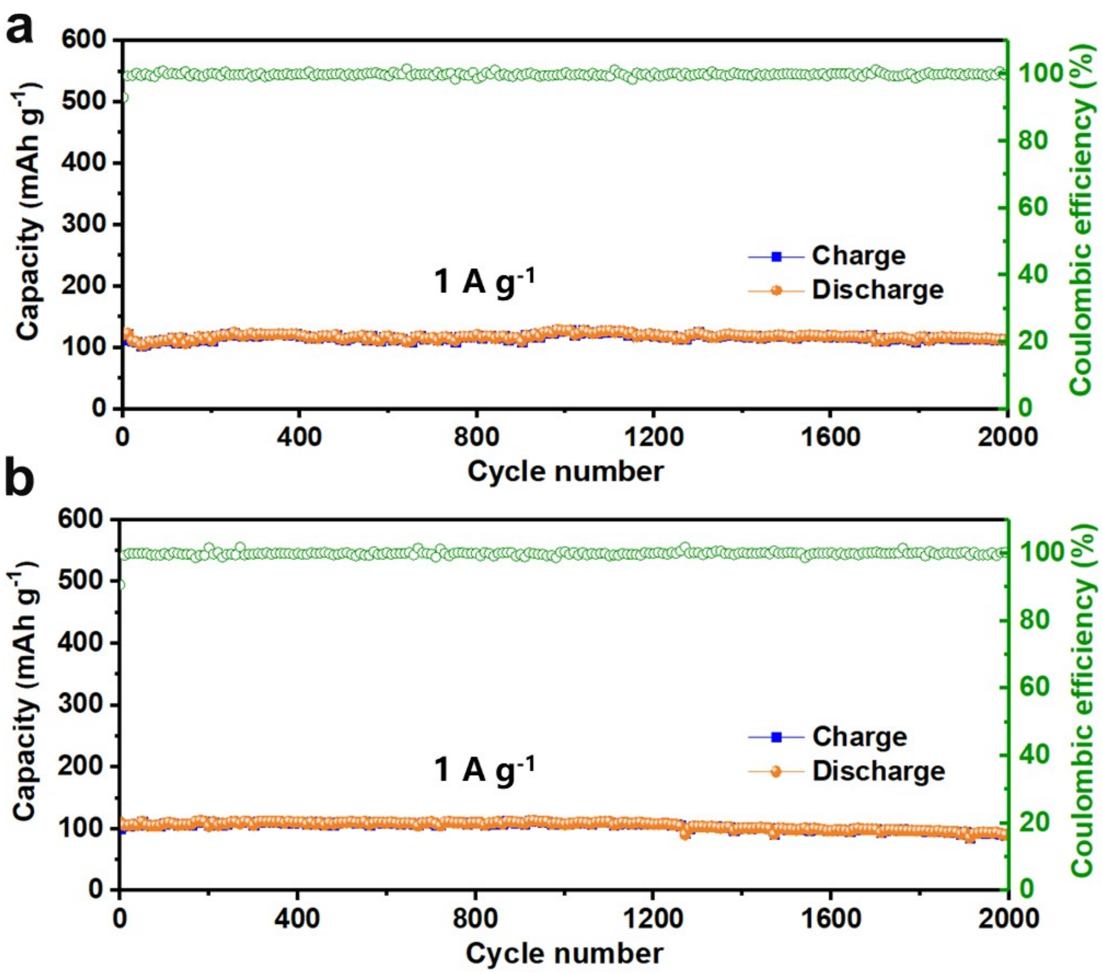

Fig. S15. Cycling performance at the current density of 1 A g^{-1} of (a) MCNP-5 and (b) MCNP-10.

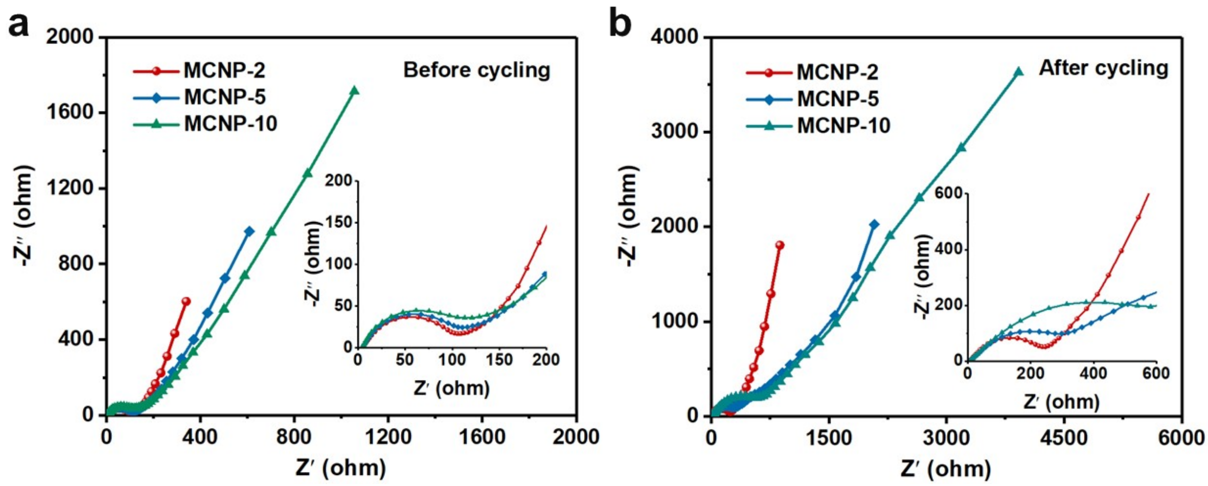

Fig. S16. Nyquist plots of the MCNPs anodes (a) before cycling and (b) after 2000 cycles at the current density of 1 A g^{-1}.

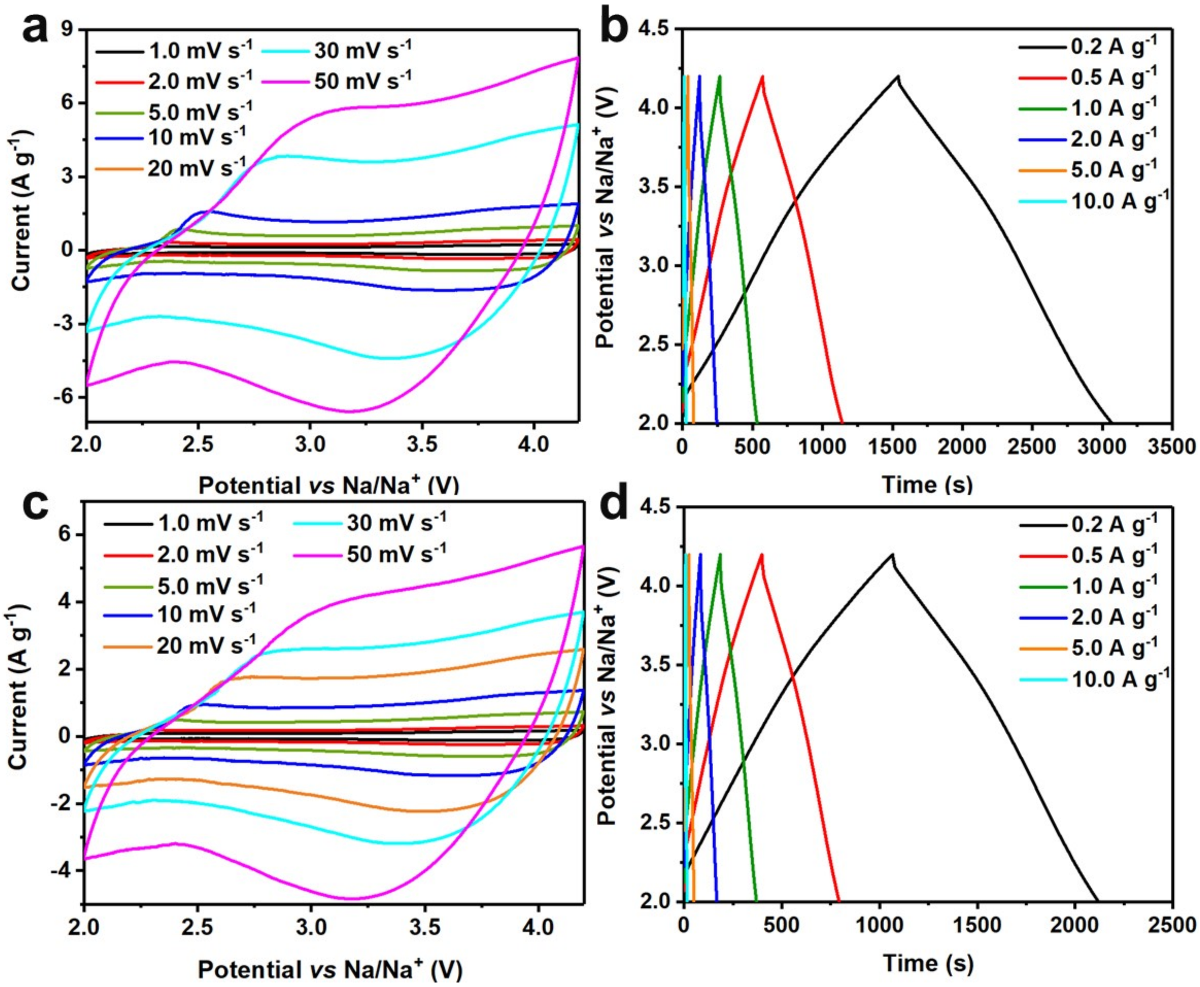

Fig. S17. CV curves of (a) HCNP-0 and (c) YP-50F at different scan rates. GCD curves of (b) HCNP-0 and (d) YP-50F at different current densities.

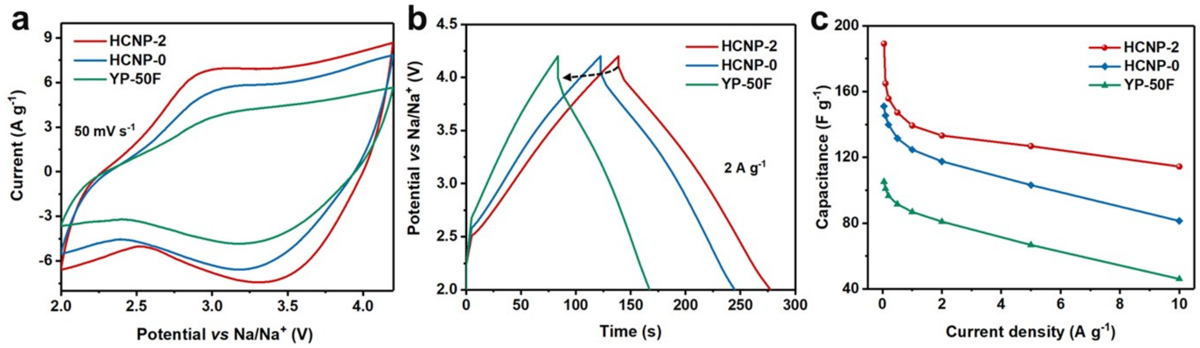

Fig. S18. (a) CV curves of HCNP-2, HCNP-0 and YP-50F at 50 mV s^{-1}. (b) GCD curves of HCNP-2, HCNP-0 and YP-50F at 2 A g^{-1}. (c) Rate performance of HCNP-2, HCNP-0 and YP-50F.

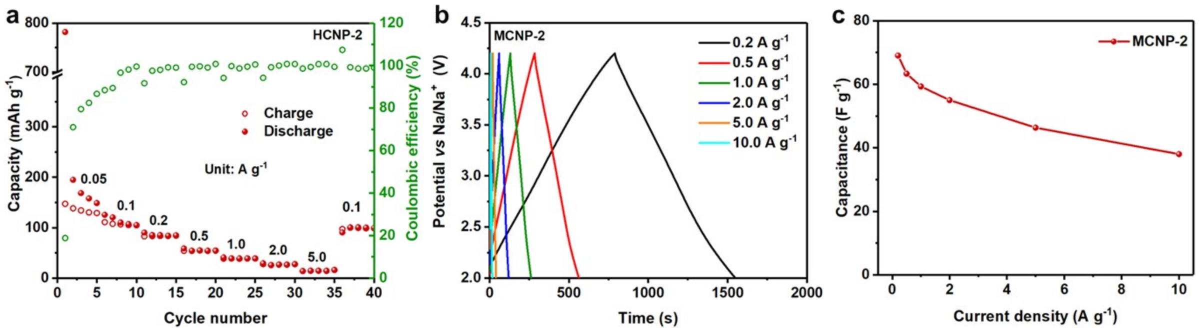

Fig. S19. (a) Rate performance of HCNP-2 anode. (b) GCD curves and (c) rate performance of MCNP-2 cathode.

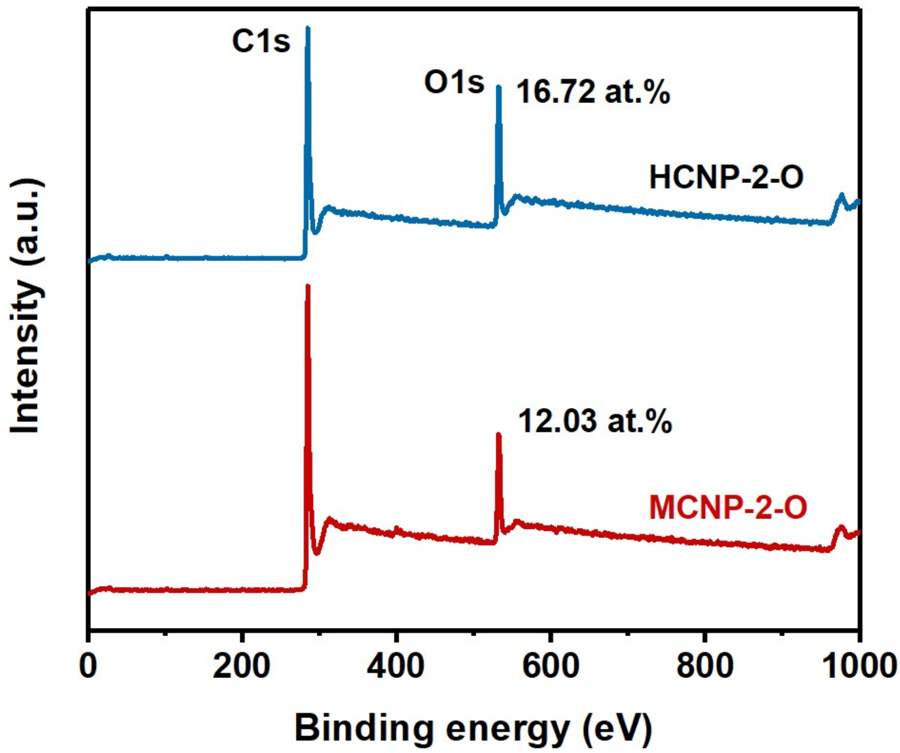

Fig. S20. XPS spectra of MCNP-2-O and HCNP-2-O.

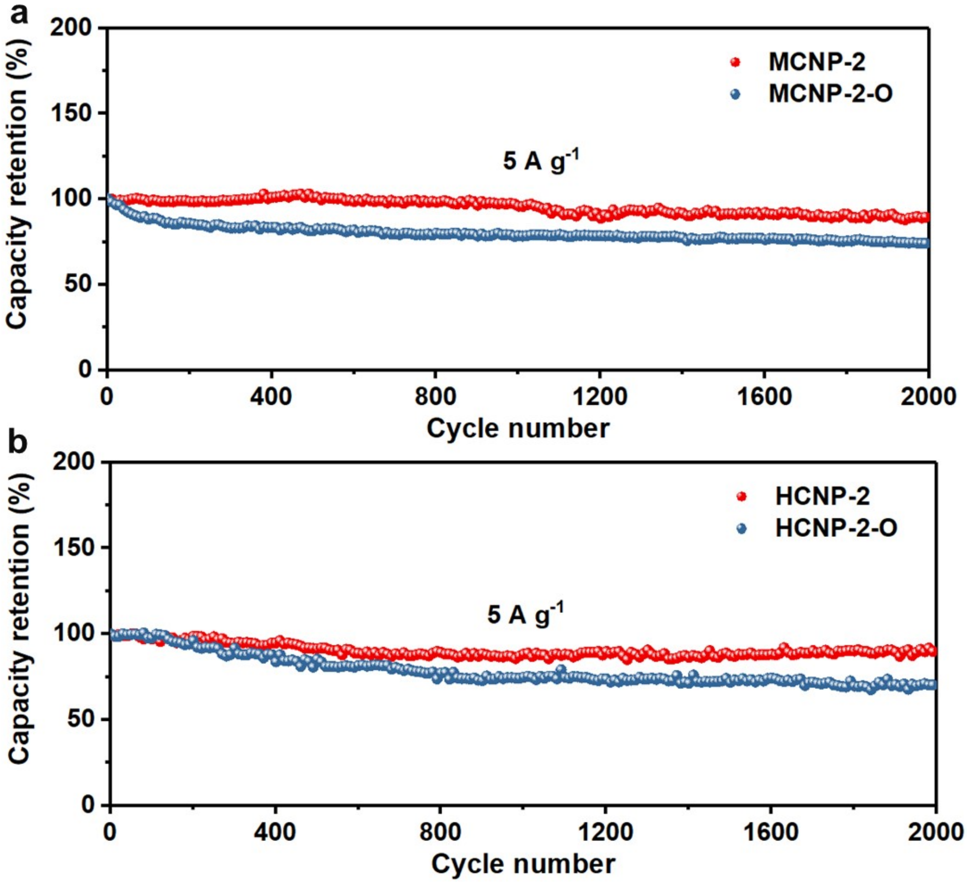

Fig. S21. Cycling performance of (a) MCNP-2, MCNP-2-O and (b) HCNP-2, HCNP-2-O.

In order to explore the effect of oxygen content on the cycling stability of electrodes, we used concentrated nitric acid treatment to increase the oxygen content in the samples. As shown in **Fig. S20**, the oxygen content of MCNP-2-O and HCNP-2-O increase from 4.03 at.% and 4.48 at.% to 12.03 at.% and 16.72 at.%, respectively. These results indicate that a large number of oxygen functional groups are introduced into the samples. The cycling performance of the obtained samples are further studied at the current density of 5 A g^{-1}. After 2000 charge/discharge cycles, MCNP-2 anode delivers a high capacity retention of 90.5%, while MCNP-2-O is only 73.7%. Similarly, HCNP-2 shows a capacity retention rate of 91.4%, which is higher than 70.1 % of HCNP-2-O (**Fig. S21**). Therefore, the high carbon content and low oxygen content for the MCNP-2 and HCNP-2 are beneficial to guarantee the long cycle stability of constructed electrodes.

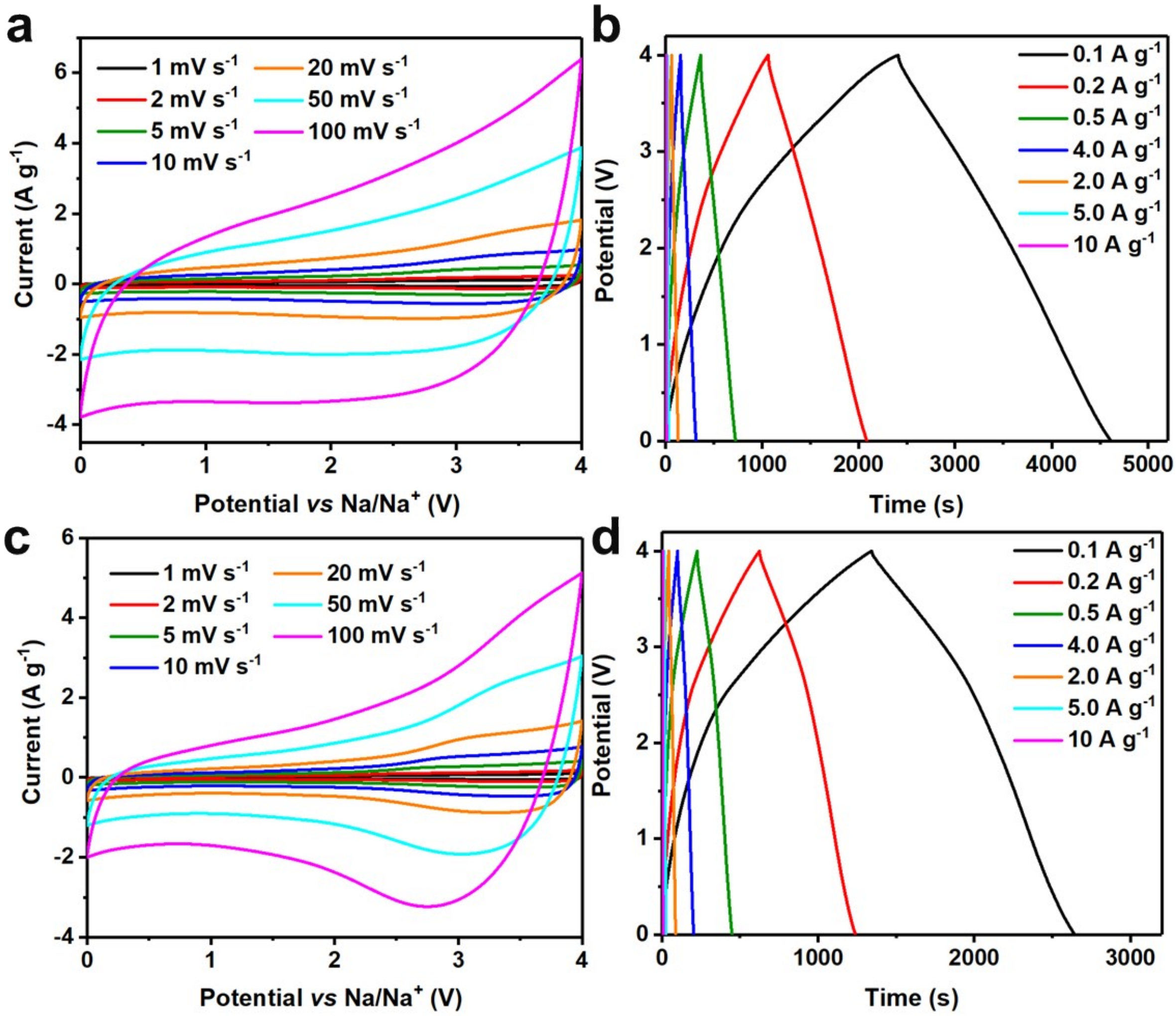

Fig. S22. CV curves of MCNP-2//HCNP-2 with different mass ratios: (a) 1:1, (c) 1:3. GCD curves of MCNP-2//HCNP-2 with different mass ratios: (b) 1:1, (d) 1:3.

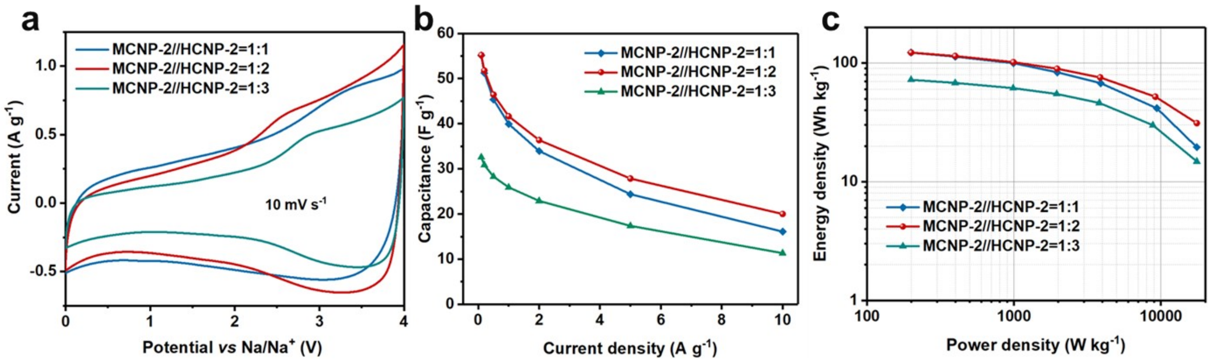

Fig. S23. (a) CV curves of MCNP-2//HCNP-2 at 10 mV s^{-1} with different mass ratios. (b) Rate performance of MCNP-2//HCNP-2 with different mass ratios. (c) Ragone plots of MCNP-2//HCNP-2 with different mass ratios.

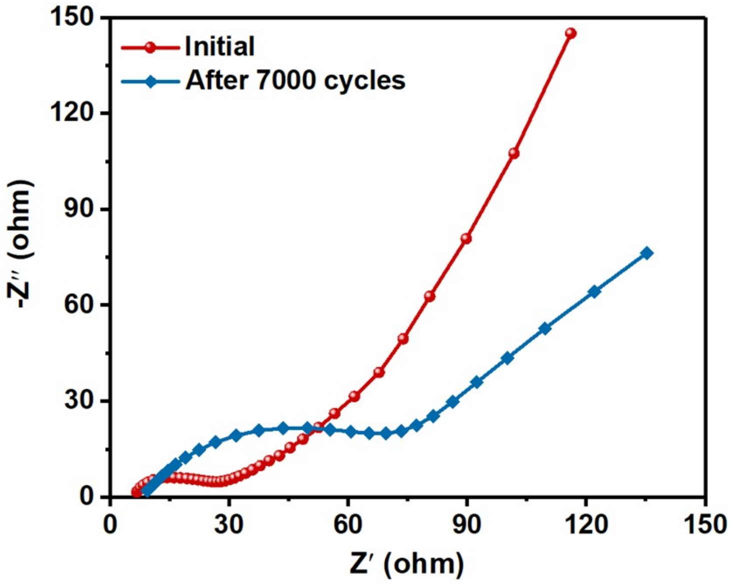

Fig. S24 Nyquist plots of the MCNP-2//HCNP-2 SIC before and after 7000 cycles at the current density of 1 A g^{-1}.

Table S1. The detailed amount of raw materials and corresponding pore structure parameters of various samples.

Samples	**Coal tar mass (g)**	**Template mass (g)**	**K_2CO_3 mass (g)**	**$^{a}S_{BET}$ (m^2 g^{-1})**	**$^{b}V_{total}$ (cm^3 g^{-1})**	**$^{c}V_{mic}$ (cm^3 g^{-1})**	**$^{d}V_{mes}+V_{mac}$ (cm^3 g^{-1})**
MCNP-2	1	2	0	793.2	2.67	0.30	2.37
MCNP-5	1	5	0	925.8	1.30	0.35	0.95
MCNP-10	1	10	0	569.4	0.68	0.23	0.45
HCNP-2	1	2	3	1530.8	3.17	0.64	2.53
HCNP-0	1	0	3	1098.0	0.82	0.52	0.30

a: The BET specific surface area. b: The total pore volume. c: Micropore (d < 2 nm) pore volume. d: The sum of mesopore and macropore pore volume.

Table S2. Comparison with the performance of previously reported SICs.

Hybrid system	Voltage Window	Energy Density/ Power Density	Current Density	Cycling Stability	Ref.
NHPC-800//NHPAC	0-4 V	115 Wh kg^{-1} at 200 W kg^{-1}	1 A g^{-1}	~40 % capacity retention after 10000 cycles	8
MCMB//AC	1-4 V	93.5 Wh kg^{-1} at 573 W kg^{-1} 86.5 Wh kg^{-1} at 2832 W kg^{-1}	20 C	60.1 % capacity retention after 3000 cycles	9
SCN//SCN-A	0-4 V	112 Wh kg^{-1} at 67 W kg^{-1} 45 Wh kg^{-1} at 12000 W kg^{-1}	5 A g^{-1}	82 % capacity retention after 3000 cycles	10
HPC-550//HPC-800	0-4 V	103.2 Wh kg^{-1} at 70 W kg^{-1} 22.3 Wh kg^{-1} at 15900 W kg^{-1}	3.5 A g^{-1}	81.1 % capacity retention after 2500 cycles	11
HC//AC	0-4.2 V	~100 Wh kg^{-1} ~7000 W kg^{-1}	2 A g^{-1}	40 % capacity retention after 10000 cycles	15
TiO_2/graphene//AC	1-3.8 V	64.2 Wh kg^{-1} at 56.3 W kg^{-1} 25.8 Wh kg^{-1} at 1357 W kg^{-1}	10 C	90 % capacity retention after 10000 cycles	16
G@mNb_2O_5//AC	0.1-2.5 V	56.1 Wh kg^{-1} at 120 W kg^{-1} 9.7 Wh kg^{-1} at 7200 W kg^{-1}	1 A g^{-1}	89 % capacity retention after 800 cycles	17
Ti(O, N)//AC	0.5-4 V	46 Wh kg^{-1} at 46 W kg^{-1} 10.9 Wh kg^{-1} at 11500 W kg^{-1}	1 A g^{-1}	85.9 % capacity retention after 500 cycles	18
$FeS_{2-x}Se_x$//AC	0.5-3.5 V	67 Wh kg^{-1} at 172 W kg^{-1} 27 Wh kg^{-1} at 2543 W kg^{-1}	1 A g^{-1}	70 % capacity retention after 3000 cycles	20
SnS_2/GCA//AC	1-4.3 V	108.3 Wh kg^{-1} at 130 W kg^{-1} 26.9 Wh kg^{-1} at 6053 W kg^{-1}	1 A g^{-1}	68.4 % capacity retention after 1500 cycles	21
$NaTi_2(PO_4)_3$/graphene// graphene	0-3 V	~80 Wh kg^{-1} ~8000 W kg^{-1}	4 A g^{-1}	90 % capacity retention after 75000 cycles	22
$NaTi_2(PO_4)_3$/rGO//AC	0-2.7 V	53 Wh kg^{-1} at 330 W kg^{-1}	1.5 A g^{-1}	93 % capacity retention after 5000	23

		31 Wh kg^{-1} at 6700 W kg^{-1}		cycles	
CS-800//CS-800-6	2-4 V	52.2Wh kg^{-1} at 300 W kg^{-1} ~3000 W kg^{-1}	1 A g^{-1}	85.7 % capacity retention after 2000 cycles	59
Nb_2O_5 NRs/NMMCNF //AC	1-4 V	91 Wh kg^{-1} at 75 W kg^{-1} 52 Wh kg^{-1} at 7499 W kg^{-1}	1 A g^{-1}	77 % capacity retention after 10000 cycles	60
TiS_2//AC	0-2.6 V	~38 Wh kg^{-1}	1 A g^{-1}	80 % capacity retention after 3600 cycles	61
3DM-GO//AC	0-4 V	~73.4 Wh kg^{-1} ~3998.3 W kg^{-1}	1 A g^{-1}	77.5 % capacity retention after 2500 cycles	62
HPCNS//HPC	0-4 V	105.2 Wh kg^{-1} at 70 W kg^{-1} 32.5 Wh kg^{-1} at 60400 W kg^{-1}	3.5 A g^{-1}	85.8 % capacity retention after 4000 cycles	63
b-NMO/C//graphite	0.5-3.8 V	91 Wh kg^{-1} at 84 W kg^{-1} 37 Wh kg^{-1} at 5816 W kg^{-1}	1 A g^{-1}	72 % capacity retention after 100 cycles	64
HC//CS-AC	1.4-3.9 V	~82 Wh kg^{-1}	1.5 A g^{-1}	60 % capacity retention after 8000 cycles	65
PI-2.5//AC(PI-5)	0-4.2 V	66 Wh kg^{-1} at 196 W kg^{-1} 13.3 Wh kg^{-1} at 1200 W kg^{-1}	0.4 A g^{-1}	65.6 % capacity retention after 500 cycles	66
MCNP-2//HCNP-2	0-4 V	122.4 W h kg^{-1} at 199.7 W kg^{-1} 31.1 W h kg^{-1} at 17.5 kW kg^{-1}	1 A g^{-1}	71 % capacity retention after 7000 cycles	This work

References

[S1] Lu, Zhiyi; Chen, Guangxu; Siahrostami, Samira; Chen, Zhihua; Liu, Kai; Xie, Jin; Liao, Lei; Wu, Tong; Lin, Dingchang; Liu, Yayuan; Jaramillo, Thomas F.; Nørskov, Jens K.; Cui, Yi. High-efficiency oxygen reduction to hydrogen peroxide catalysed by oxidized carbon materials. Nature Catalysis 2018, 1, 2, 156-162.

[S2] Chen, Wei; Li, Kaixu; Xia, Mingwei; Yang, Haiping; Chen, Yingquan; Chen, Xu; Che, Qingfeng; Chen, Hanping. Catalytic deoxygenation co-pyrolysis of bamboo wastes and microalgae with biochar catalyst. Energy 2018, 157, 472-482.